Zhou and Chen
Advances in Bridge Engineering (2024) 5:1
https://doi.org/10.1186/s43251-023-00112-2

Advances in
Bridge Engineering

ORIGINAL INNOVATION

Open Access

A hybrid approach for fatigue assessment of reinforced concrete bridge deck considering realistic bridge-traffic interaction

Yufen Zhou[1] and Suren Chen[2*]

*Correspondence:
srchen@seu.edu.cn; suren.chen@colostate.edu

[1] Former Postdoctoral Fellow, Ph.D., Dept. of Civil & Environmental Engineering, Colorado State University, Fort Collins, CO 80523, USA
[2] Department of Bridge Engineering, College of Transportation, Southeast University, Nanjing, China

Abstract

Reinforced concrete (RC) bridge decks are directly exposed to daily traffic loads and often experience surface cracking caused by excessive stress or fatigue accumulation. The bridge deck fatigue performance over traffic loads needs to be assessed based on accurate dynamic interaction analysis of the bridge and realistic moving vehicles. Most of existing studies on fatigue assessment focus on either the bridge global response without sufficient details about the bridge deck, or refined bridge deck modeling without considering the full dynamic interaction between moving traffic and the bridge structure realistically. A hybrid fatigue assessment approach is developed by combining mode-based global bridge-traffic dynamic interaction analysis, finite-element (FE)-based refined bridge deck model, and fatigue assessment method directly based on the vehicle loads and shear strength of the bridge deck. The proposed approach is demonstrated with a typical 3-span concrete bridge under realistic traffic and road surface conditions. Based on the dynamic interaction and stress analysis results, the fatigue damage factor is further investigated with different road surface roughness levels and heavy truck proportions. It is found that the proposed analytical approach provides a useful tool to predict the bridge deck response and potential fatigue damage under realistic traffic flow.

Keywords: Highway bridge, Bridge deck, Traffic, Bridge vehicle interaction, Dynamic response, Fatigue

1 Introduction

Highway bridges support increasing daily traffic due to the growth of social, economic, and recreational needs of the society. Typical highway bridges, mostly in the form of multi-span reinforced concrete (RC) bridges, gradually deteriorate due to the presence of traffic during their lifespans. One important vulnerability of a highway bridge is its cumulative fatigue damage on the bridge components such as the bridge deck when the bridge ages. The traffic load was traditionally considered as design live loads with dynamic amplification factors for fatigue assessment of highway bridges. Not until recently, studies have indicated that the dynamic effects between a bridge and vehicles cannot be completely captured unless the vehicles are modeled as dynamic systems

along with the vibrating bridge. On the one hand, vibrating heavy road vehicles may significantly change the local and global dynamic behavior and affect the fatigue life of the bridge. On the other hand, the vibration of the bridge may in turn affect the dynamic performance of the vehicles, which may pose significant influence on the vehicle safety and comfort of the passengers. Nowadays, the weigh-in-motion data has revealed that with an increasing demand of freight transportation to meet the increasing social needs, the number of heavy vehicles increases every year at a constantly growing speed. This would make the accurate prediction of the fatigue damage on the bridge more critical and challenging.

To meet the challenges highway bridges are currently experiencing, the proper consideration of bridge-vehicle dynamic interactions becomes essential to a rational bridge fatigue assessment. The investigation of bridge vibrations under moving vehicles has been traditionally conducted by considering only a single vehicle by treating as a moving load (Olsson 1991), moving mass (Lee 1996), or moving sprung mass (Yang and Wu 2001). It has long been observed that when a bridge is subjected to moving vehicle loads, the induced dynamic deflections and stresses can be significantly higher than those only considering the static load effects of vehicles (Yang and Yau 1997). The dynamic interaction between passing vehicles and the bridge may be even more significant when increasing traffic volume is involved. Most of the existing studies dealt with the interactions between bridge and a single vehicle or a series of vehicles at certain intervals moving through the bridge at constant speeds (Xu and Guo 2003; Cai and Chen 2004). Nevertheless, considering that the traffic on a typical bridge is stochastic following certain rules, e.g., accelerating, decelerating, and braking, the interactions between the bridge and vehicles may be largely different from those with a series of vehicles driven at equal intervals at constant speeds. Chen and Wu (2010) proposed a simulation methodology to evaluate the bridge dynamic performance considering the combined effects of wind and stochastic traffic from the bridge-single-vehicle interaction analysis (Chen and Cai 2007). Such an approach (Chen and Wu 2010), however, did not couple all the vehicles and the bridge simultaneously therefore the dynamic interaction effects from multiple vehicles cannot be considered at the same time. Fully coupled bridge-traffic interaction analysis has been proposed by Zhou and Chen (2015) for long-span bridges to consider the combined effects from wind and traffic. However, the approach focuses on global nonlinear iterative dynamic analysis and is not compatible with most commercial finite element software, which may be needed when detailed deck modeling is required.

Most existing studies on fatigue assessment of multi-span highway bridges considered vehicle loads based on single-vehicle analyses (MacDougall et al. 2006; Wu et al. 2012; Deng et al. 2020). Therefore, the effect from the presence of multiple vehicles in realistic traffic flow on the bridge cannot be incorporated. Luo et al. (2021) used weigh-in-motion (WIM) data to consider stochastic traffic flow in fatigue reliability evaluation. However, the dynamic interaction effects between the bridge and stochastic traffic flow with realistic vehicle speed and location cannot be considered. The fatigue assessment considering realistic traffic flow effects, such as interaction of bridge and multiple vehicles, vehicle behavior following common traffic rules, is not found in the existing literature. To bridge this gap, this study presents a hybrid approach to assess the fatigue performance of bridge deck on multi-span highway bridges under normal stochastic

traffic flow. Such a hybrid approach consists of the refined finite element model of the bridge and fully coupled bridge-traffic interaction model using modal coordinates, and fatigue assessment method based on the vehicle loads and shear strength of the bridge deck. Taking advantage of the strength of commercial software for detailed bridge deck modeling and a mode-based bridge-traffic model for coupled interaction effects, the presented model can directly consider dynamic interactions of the bridge and multiple vehicles in the traffic flow through the equivalent moving traffic load (EMTL) as joint loads. In addition, instead of using a codified S-N curve based on stress range on the bridge deck like most existing studies did, the present study uses an experimentally determined S-N curve based on the vehicle load and shear strength on a typical reinforced concrete deck, which enables the direct use of the EMTL from bridge-traffic interaction analysis. The approach to conduct the hybrid interaction analysis and further calculate the fatigue damage factor is presented and demonstrated on a prototype multi-span highway bridge, after which the effects of the road surface roughness and heavy truck proportion on the fatigue damage factor are investigated parametrically.

2 The hybrid fatigue assessment model

The formulation of bridge-vehicle interaction is dependent on the instantaneous response of the bridge and each individual vehicle. Therefore, the dynamic analysis needs to iteratively proceed, which presents a challenge for common commercial finite element (FE) programs since the built-in modules of the FE programs are usually hard to incorporate dynamic iterative analysis functions. However, commercial finite element programs have advantages in various finite element formulations and advanced meshing options, which makes them good candidates for the detailed modeling of the bridge deck of a multi-span highway bridge. The hybrid bridge dynamic model combines the finite element bridge model and the mode-based bridge-traffic interaction model. In the mode-based bridge-traffic interaction model, the bridge is modeled using modal coordinates and the vehicles are modeled using physical coordinates. The global dynamic responses (e.g., displacement) of the bridge and each individual vehicle can be obtained through the mode-based interaction analysis in time domain, from which the equivalent wheel loads from moving vehicles are derived. The equivalent wheel loads are then applied on the joints of the bridge deck in the finite element model to consider the effect of moving traffic. For the bridge deck performance assessment, the popular plate bending theory and fatigue assessment methodology are adopted, with which the detailed bridge deck response including strain, stress and internal forces can be obtained through the finite element shape functions, and the fatigue performance is further assessed. The hybrid fatigue assessment model can be illustrated in the following flow chart (Fig. 1) and the detailed modeling process is introduced in the following Sections.

2.1 Refined-scale bridge finite element model using SAP2000

To accurately represent the 3-D bridge behavior, bridge deck is usually modeled using plate model or grillage model. Plate bridge models have been used to investigate the bridge dynamic performance under moving vehicles, as demonstrated in several studies (Olsson 1985; Zhu and Law 2002; González et al. 2010). Alternatively, grillage bridge models are also found in the literature for bridge dynamic analysis considering

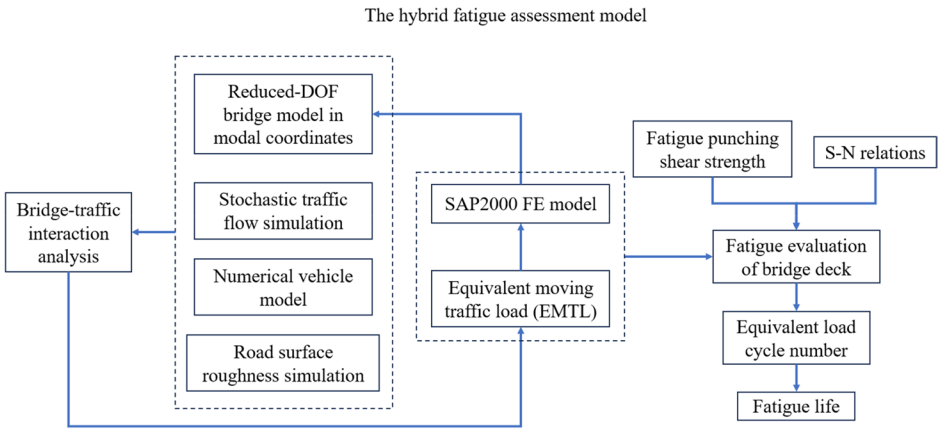

Fig. 1 Illustration of the hybrid fatigue assessment model using flowchart

interactions with moving vehicles, as seen in some references (Huang et al. 1992; Nassif and Liu 2004). In the grillage bridge model, the bridge deck is discretized as skeletal structure consisting of a mesh of 1-D beam elements. Despite some advantages in terms of simplicity and computational efficiency, the grillage modeling of bridge deck is approximate due to failing to capture some details of the bridge deck which are essential to damage and fatigue assessment. For instance, the internal force is discontinuous at the grillage nodes for a normal mesh. In the present study, the plate bridge model is adopted for bridge deck modeling of the multi-girder highway bridge. Commercial finite element software SAP2000 is a popular finite element modeling and analysis tool which is widely used in design, static and dynamic analysis of bridge and building structures, and is therefore adopted herein to develop the refined-scale bridge finite element model.

2.2 Traffic modeling

2.2.1 Stochastic traffic flow simulation

In this study, the three-lane cellular automaton model is adopted to simulate the instantaneous behavior of vehicles both temporally and spatially. As a mathematical idealization of physical systems with discrete time and space, cellular automaton consists of a finite set of discrete variables to represent specific vehicle information. The discrete variables for individual vehicle include the vehicle occupied lane, vehicle longitudinal location, vehicle type, vehicle speed, vehicle driving direction. The variables in each cellular are updated based on the vehicle information in the adjacent locations and the probabilistic traffic rules regulating the accelerating, decelerating, lane changing and braking maneuvers. Detailed traffic rules involved in the traffic flow simulation can be referred to the published paper (Chen and Wu 2010). The cellular automaton-based traffic flow simulation is performed on a roadway-bridge-roadway system to simulate the stochastic traffic flow through the bridge in a realistic way. The randomization of the traffic flow is realized by the stochastic initial variables in the cellular of the whole system. Periodic boundary conditions are adopted in the traffic flow model, in which the total number of each type of vehicles in the system remains

constant. The vehicles in the stochastic traffic are categorized into three types from a variety of vehicle configurations, which are heavy truck with one trailer, light truck, and light car. The vehicle classification ratio indicating the percentage for each type of vehicle is typically prescribed based on the site-specific traffic data if available.

2.2.2 Numerical vehicle model

The vehicles are modeled as a combination of several rigid bodies, wheel axles, springs, and dampers, of which the main rigid bodies are modeled to represent the vehicle bodies. The suspension system of each axle is modeled as the upper springs and the elastic tires are modeled as lower springs. Viscous dampers are adopted to model the energy dissipation system. The mass of the suspension system is assumed to be concentrated on each wheel axle while the mass of the springs and dampers are assumed to be zero. Four degrees of freedom are accompanied with the main rigid body, including two translational and two rotational degrees of freedom. The constraint equations are applied in deriving the vehicle matrices for the heavy truck model in which a pivot is used to connect the truck tractor and trailer. The numerical dynamic model for the heavy truck consists of two main rigid bodies, three-wheel axle sets, 24 sets of springs and dampers in either vertical or lateral direction, as shown in Fig. 2. The displacement vector d_v for the heavy truck model contains 19 degrees of freedom including 8 independent vertical, 8 lateral and 3 rotational degrees of freedom, which is demonstrated in Eq. (1).

$$d_v = \{Z_{r1}\ \theta_{r1}\ \beta_{r1}\ Z_{r2}\ \beta_{r2}\ Z_{a1L}\ Z_{a1R}\ Z_{a2L}\ Z_{a2R}\ Z_{a3L}\ Z_{a3R}\ Y_{r1}\ Y_{r2}\ Y_{a1L}\ Y_{a1R}\ Y_{a2L}\ Y_{a2R}\ Y_{a3L}\ Y_{a3R}\} \tag{1}$$

in which, Z_{ri} represents the vertical displacement of the i^{th} rigid body; θ_{ri} represents the rotational displacement of the i^{th} rigid body in the x-z plane; β_{ri} represents the rotational displacement of the i^{th} rigid body in the y-z plane; $Z_{aiL(R)}$ represents the vertical displacement of the i^{th} wheel axle in the left (right) side; Y_{ri} represents the lateral displacement of the i^{th} rigid body; $Y_{aiL(R)}$ represents the lateral displacement of the i^{th} wheel axle in the left (right) side. The springs and dampers are labeled according to the related axle number, upper-lower orientation, y-z direction, and left-right location, which are corresponding to the superscript and three subscripts in sequence in the notation of each stiffness coefficient K or damping coefficient C.

The numerical dynamic model for the light truck consists of one main rigid body, two-wheel axle sets, 16 sets of springs and dampers vertically or laterally. The front view of the light truck and bus is shown in Fig. 3. The side view of the numerical model for the light truck and bus is same as the one shown in Fig. 2 (b) and hereby not repeated. The displacement vector d_v for the light truck is constituted of 12 degrees of freedom including 5 independent vertical, 5 lateral and 2 rotational degrees of freedom, as demonstrated in Eq. (2).

$$d_v = \{Z_{r1}\ \theta_{r1}\ \beta_{r1}\ Z_{a1L}\ Z_{a1R}\ Z_{a2L}\ Z_{a2R}\ Y_{r1}\ Y_{a1L}\ Y_{a1R}\ Y_{a2L}\ Y_{a2R}\} \tag{2}$$

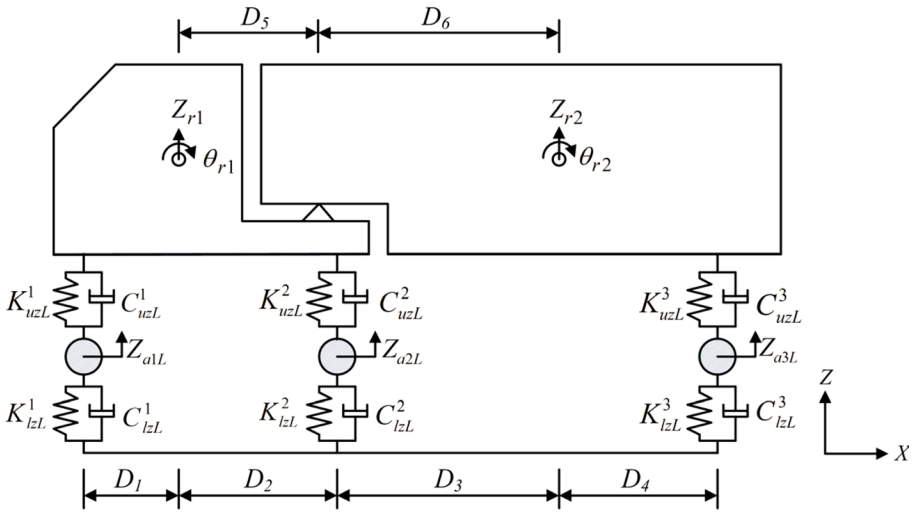

(a) Elevation view

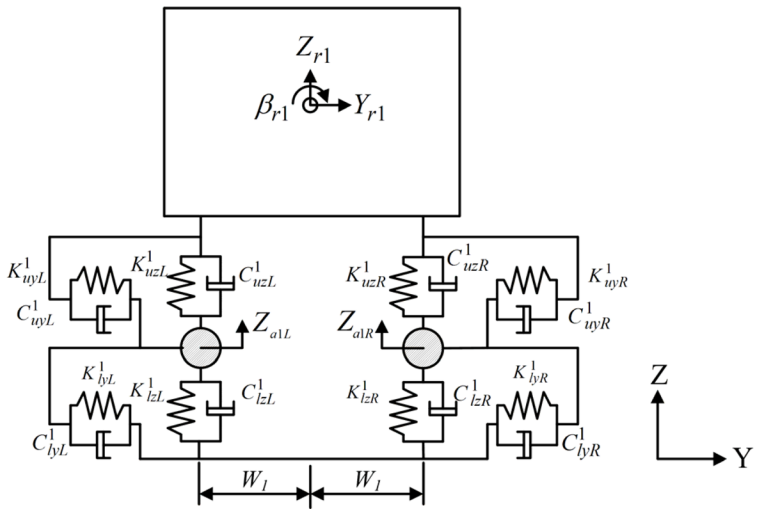

(b) Side view

Fig. 2 The numerical dynamic model for the heavy truck with one trailer

The numerical model for the light car is similar to the model for the light truck except that the vehicle dimensions and mass properties require different parameter inputs. The input data for the vehicle models includes the mass and mass moment inertia of each rigid body, the mass of each wheel axle set, the stiffness coefficient of each spring, the damping coefficient of each damper and the vehicle dimensions.

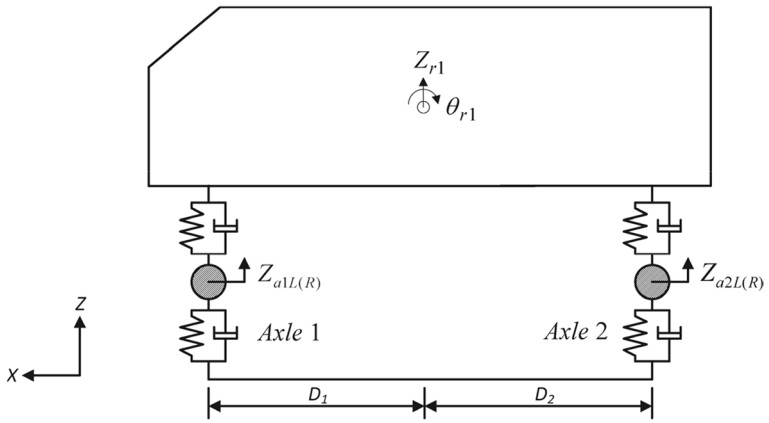

Fig. 3 Elevation view for the numerical model of the light truck and light car

2.3 Bridge-vehicle interaction analysis

2.3.1 Reduced-DOF bridge model based on modal coordinates

Like most commercial software, SAP2000 cannot directly couple the bridge and moving vehicle models to conduct the bridge-traffic dynamic interaction analysis subject to various roughness excitations. The most applicable approach is to generate equivalent nodal time-history excitation inputs of wheel loadings from passing vehicles. The multi-mode reduced-order bridge dynamic model has been used widely in the bridge dynamic analysis under wind, seismic or other dynamic loads such as vehicles. After the detailed FEM model of the bridge is developed, modal analysis is conducted to extract the first couple critical modes to the bridge dynamic response. With the selected critical modes, a reduced-DOF bridge dynamic model is developed, which can capture the dynamic response of the whole bridge with reasonable accuracy by incorporating only limited modes (Xu and Guo 2003; Chen and Cai 2007).

2.3.2 Formulation of bridge-vehicle interaction analysis

Based on the reduced-order bridge model, the coupled dynamic interaction model of a typical bridge and any number of moving vehicles subjected to road roughness profile excitations can be developed, the motion equations of which can be expressed in Eq. (3) (Zhou and Chen 2015).

$$\begin{bmatrix} M_b & 0 & 0 & 0 \\ 0 & M_{v_1} & 0 & 0 \\ 0 & 0 & \ddots & 0 \\ 0 & 0 & 0 & M_{v_n} \end{bmatrix} \begin{Bmatrix} \ddot{U}_b \\ \ddot{U}_{v_1} \\ \vdots \\ \ddot{U}_{v_n} \end{Bmatrix} + \begin{bmatrix} C_b + \sum_{i=1}^{n} C_{bci} & C_{b,v_1} & \cdots & C_{b,v_n} \\ C_{v_1,b} & C_{v_1} & 0 & 0 \\ \vdots & 0 & \ddots & 0 \\ C_{v_n,b} & 0 & 0 & C_{v_n} \end{bmatrix} \begin{Bmatrix} \dot{U}_b \\ \dot{U}_{v_1} \\ \vdots \\ \dot{U}_{v_n} \end{Bmatrix} + \begin{bmatrix} K_b + \sum_{i=1}^{n} K_{bci} & K_{b,v_1} & \cdots & K_{b,v_n} \\ K_{v_1,b} & K_{v_1} & \cdots & 0 \\ \vdots & \vdots & \ddots & \vdots \\ K_{v_n,b} & 0 & \cdots & K_{v_n} \end{bmatrix} \begin{Bmatrix} U_b \\ U_{v_1} \\ \vdots \\ U_{v_n} \end{Bmatrix} = \begin{Bmatrix} \sum_{i=1}^{n} {F_{v_1}}^G + {F_b}^r \\ {F_{v_1}}^r \\ \vdots \\ {F_{v_n}}^r \end{Bmatrix} \tag{3}$$

in which, M_b, K_b and C_b are the generalized mass, stiffness and damping matrices for the bridge structure, respectively; n is the number of vehicles travelling on the roadway-bridge-roadway system in the traffic flow; M_{v_i}, K_{v_i} and C_{v_i} are the mass, stiffness and

damping matrices of the i^{th} vehicle in the traffic flow, respectively; K_{bci} and C_{bci} refer to the stiffness and damping contributions to the bridge structure due to the coupling effects between the i^{th} vehicle in the traffic flow and the bridge system, respectively; K_{b,v_i} and C_{b,v_i} are the coupled stiffness and damping matrices contributing to bridge vibration from the i^{th} vehicle in the traffic flow, respectively; $K_{v_i,b}$ and $C_{v_i,b}$ are the coupled stiffness and damping matrices contributing to the vibration of the i^{th} vehicle in the traffic flow from the bridge structure; U_b is a vector of generalized coordinates of the bridge corresponding to each mode involved in the analysis; U_{v_i} is a vector of the physical responses corresponding to each degree of freedom of the i^{th} vehicle in the traffic flow; one-dot and two-dot superscripts of the displacement vector denote the velocity and acceleration, respectively; F_b and F_{v_i} denote the externally applied loads for the bridge in modal coordinates and the i^{th} vehicle in physical coordinates, respectively. The superscripts r and G denote the loads due to road roughness and self-weight, respectively.

2.3.3 Modeling of road surface roughness with progressive deterioration

The road surface roughness on the approaching road and the bridge deck is modeled as a stationary Gaussian random process with zero mean value. The road surface roughness r can be generated by the spectral representation formulation, which was firstly introduced by Shinozuka and Jan (1972) and expressed in Eq. (4).

$$r(x) = \sum_{i=1}^{n} \sqrt{2S\left(\overline{\varphi}_k\right)\Delta\overline{\varphi}} \cos\left(2\pi\overline{\varphi}_k x + \theta_k\right) \tag{4}$$

in which, n is the number of points in the inverse Fourier Transform; x is the location on the road surface; θ_k is the random phase angle with a uniform distribution between 0 and 2π; ϕ is the power spectral density function, which adopts the formation suggested by Huang et al. (1992).

$$\varphi(n) = \varphi(n_0)\left(\frac{n}{n_0}\right)^{-2} \tag{5}$$

in which, n is the spatial frequency (cycle/m); n_0 is the discontinuity frequency of $1/2\pi$ (cycle/m); $\phi(n_0)$ is the road roughness coefficient (m^3/cycle).

The road roughness coefficient is predicted using the international roughness index (IRI) (Shiyab 2007).

$$\varphi(n_0) = 6.1972 \times 10^{-9} \times e^{(IRI/0.42808)} + 2 \times 10^{-6} \tag{6}$$

The IRI values at time t can be calculated using the following equation (Paterson 1986)

$$IRI = 1.04e^{\eta t} IRI_0 + 263(1 + SNC)^{-5}(CESAL)_t \tag{7}$$

in which, IRI_0 is the initial roughness value; t is time in years; η is the environmental coefficient; SNC is the structural number; $(CESAL)_t$ is the estimated number of traffic at time t in million.

The road roughness coefficient in a 15-year period can be calculated as follows in Eq. (8) (Dodds 1972).

$$\varphi(n_0) = \left\{ \begin{array}{l} 5 \times 10^{-6} very\ good\ condition\ when\ t \le 10 years \\ 20 \times 10^{-6}\ good\ condition\ when\ 11 \le t \le 12 years \\ 80 \times 10^{-6}\ average\ condition\ when\ t \le 13 years \\ 320 \times 10^{-6} poor\ condition\ when\ 14 \le t \le 15 years \end{array} \right\} \tag{8}$$

2.4 Equivalent moving traffic load (EMTL)

The equivalent wheel loads (EWL) can be obtained directly for each vehicle in the stochastic traffic flow from the time-history simulation results of the fully coupled bridge-traffic interaction analysis. Based on the instantaneous location of each vehicle in the traffic flow, the vertical equivalent moving traffic loads (EMTL) for the bridge girder joints are further accumulated by distributing the EWL for each vehicle linearly to the adjacent bridge girder joints both longitudinally and laterally. EMTL will then be applied on the bridge as the time-history joint loads to consider the effect from moving traffic.

The vertical equivalent wheel load for the i^{th} vehicle is determined as the summation of the vertical equivalent dynamic wheel loads (EDWL) and the gravity loads as expressed in Eq. (9).

$$F_{ewl}^{iz}(t) = F_{edwl}^{iz}(t) + G^i \tag{9}$$

in which, G^i is the gravity load of the i^{th} vehicle; $F_{edwl}^{iz}(t)$ is the vertical dynamic wheel loads for the i^{th} vehicle in the traffic flow at time instant t, which are defined as (Chen and Cai 2007):

$$F_{edwl}^{iz}(t) = \sum_{j=1}^{na} \left(K_{lzL}^{j} \hat{Z}_{ajL}(t) + C_{lzL}^{j} \dot{\hat{Z}}_{ajL}(t) + K_{lzR}^{j} \hat{Z}_{ajR}(t) + C_{lzR}^{j} \dot{\hat{Z}}_{ajR}(t) \right) \tag{10}$$

in which, $\hat{Z}_{ajL(R)}(t)$ and $\dot{\hat{Z}}_{ajL(R)}(t)$ are the relative vertical displacements and the corresponding first derivatives between the lower mass block on the vehicle at the left (right) side and the contacting point on the bridge, respectively; *na* is the total number of wheel axles for the i^{th} vehicle; K and C are the stiffness and damping coefficients of the springs and dampers in the vehicle model, respectively; the subscripts *l*, *z*, *L(R)* represent lower position, vertical (z) direction and left (right) side for the springs or dampers, respectively.

The corresponding vertical equivalent wheel loads for the i^{th} vehicle in the p^{th} modal coordinate of the bridge subsystem can be expressed in the following equation.

$$\begin{aligned} F_{ewl}^{piz}(t) = & \sum_{j=1}^{na} \left(K_{lzL}^{j} \hat{Z}_{ajL}(t) + C_{lzL}^{j} \dot{\hat{Z}}_{ajL}(t) + G_j^i \right) \left(h_j^{pi}(t) + d_{jL}^{i}(t) \alpha_j^{pi}(t) \right) + \\ & \sum_{j=1}^{na} \left(K_{lzR}^{j} \hat{Z}_{ajR}(t) + C_{lzR}^{j} \dot{\hat{Z}}_{ajR}(t) + G_j^i \right) \left(h_j^{pi}(t) + d_{jR}^{i}(t) \alpha_j^{pi}(t) \right) \end{aligned} \tag{11}$$

in which, G_j^i is the gravity load at the j^{th} axle of the i^{th} vehicle; $h_j^{pi}(t)$ and $\alpha_j^{pi}(t)$ are p^{th} modal coordinates in the vertical and rotational directions for the j^{th} axle of the i^{th} vehicle at time instant t, respectively; $d_{jL}^{i}(t)$ and $d_{jR}^{i}(t)$ are the transverse distances to the centerline for the j^{th} axle of the i^{th} vehicle at the left and right sides, respectively.

2.5 Fatigue evaluation of reinforced concrete (RC) decks

2.5.1 Punching shear strength and fatigue punching shear strength

The fatigue assessment adopts the theory proposed by Matsui (1984) and Perdikaris and Beim (1988), which stresses that the bridge decks may fail under concentrated wheel loads through punching shear failure. Punching shear strength of the bridge deck V_{ps} is expressed as:

$$V_{ps} = \tau_{s\max}[2(a+2x_m)x_d + 2(b+2x_d)x_m] + \sigma_{t\max}[2(4C_d + 2d_d + b)C_m + 2(a+2d_m)C_d] \tag{12}$$

in which, a is the length of the loaded area in the bridge transverse direction; b is the length of the loaded area in the bridge longitudinal direction; x_m and x_d are neutral axis depths measured from the top surface of the bridge deck in the bridge transverse and longitudinal direction, respectively; d_m and d_d are effective depths of longitudinal and transverse bars, respectively; C_m and C_d are concrete covers of transverse and longitudinal bars, respectively; B is the effective width, $B = b + 2d_d$. τ_{smax} and σ_{smax} are the maximum shear and normal stress of concrete, respectively, which are expressed in the following equations.

$$\tau_{s\max} = 0.252f_c^{'} - 0.00251f_c^{'} \tag{13}$$

$$\sigma_{t\max} = 0.269\left(f_c^{'}\right)^{2/3} \tag{14}$$

in which, $f_c^{'}$ is compressive strength of concrete.

Matsui (1984) also proposed that fatigue punching shear strength P_{f0} can be calculated as:

$$P_{f0} = 2B(\tau_{s\max}x_m + \sigma_{t\max}C_m) \tag{15}$$

2.5.2 S-N relations

The S-N relations of reinforced concrete decks are developed by Matsui (1984) through repeated load tests. In the study by Matsui (1984), a series of dry and wet reinforced

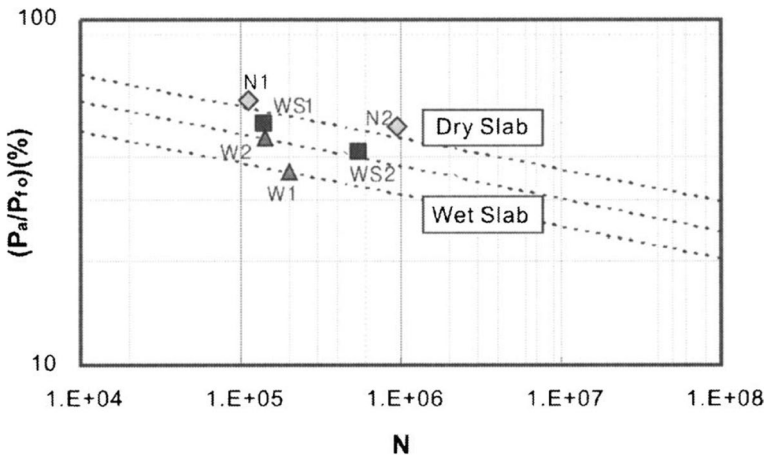

Fig. 4 Logarithm plots of S-N relations from repeated load tests of reinforced concrete slabs under moving wheel loads (Matsui 1984)

concrete slabs are tested under moving wheel loads to determine the relations between load level S and cycles-to-fatigue N. The test results are demonstrated in Fig. 4.

The S-N relation for dry RC slab is expressed as

$$\log S + C_1 \log N = \log C_2 \tag{16}$$

in which, $S = P_a/P_{f0}$; P_a is the applied shear load; P_{f0} is the fatigue punching shear strength; $C_1 = 0.0784$; $C_2 = 1.52$.

The cycles-to-fatigue can be expressed as

$$N = 10^{1/C_1(\log C_2 - \log S)} \quad \text{or} \quad \mathrm{N} = \left(\frac{\mathrm{C_2}}{\mathrm{S}}\right)^{1/\mathrm{C_1}} \tag{17}$$

2.5.3 Equivalent load cycle number N_{eq} and the fatigue life

According to the S-N curves for the bridge concrete deck under vehicle wheel loads, the bridge deck fails at different number of load cycles under different applied shear loads. Suppose that the bridge deck fails at N_1 and N_2 load cycles under applied shear load P_1 and P_2, respectively, the following relations can be obtained.

$$\log\left(P_1/P_{f0}\right) + C_1 \log N_1 = \log C_2 \tag{18a}$$

$$\log\left(P_2/P_{f0}\right) + C_1 \log N_2 = \log C_2 \tag{8b}$$

which will give,

$$P_1/P_{f0} \cdot N_1^{C_1} = C_2 \tag{19a}$$

$$P_2/P_{f0} \cdot N_2^{C_1} = C_2 \tag{19b}$$

By dividing Eqs. (19a &b) on both the left and right sides, the fatigue shear strength P_{f0} will be eliminated and the relation between the numbers of load cycles N_1 and N_2 can be obtained:

$$N_1 = \left(\frac{P_2}{P_1}\right)^{1/C_1} N_2 \tag{20}$$

The fatigue damage is assumed to be accumulated in a linear mechanism and Miner's rule is applied to calculate the equivalent number of load cycles N_{eq}. Supposing the bridge deck fails at N_{basic} cycles under the applied load P_{basic}, the equivalent number of load cycles N_{eq} during certain time period t_0 seconds corresponding to the example applied load P_{basic} can be expressed as (Oh et al. 2007),

$$N_{eq,t_0} = \sum_{i=1}^{n} \left(P_i/P_{basic}\right)^{1/C_1} N_i \tag{21}$$

in which, P_i and N_i are the applied shear load and number of cycles at different load levels during time period t_0, respectively; n is the total number of load levels during time period t_0.

Fatigue damage factor γ_0 for 1 hour is obtained using the following equation:

$$\gamma_0 = \frac{N_{eq,t_0}}{N_{basic}} \cdot \frac{60 \cdot 60}{t_0} \tag{22}$$

The bridge deck is considered to reach fatigue life if γ_0 reaches 1.0.

3 Numerical analysis on the prototype bridge under a typical traffic condition

3.1 The prototype highway bridge

3.1.1 Bridge parameters

The prototype multi-span highway bridge has three continuous spans in the longitudinal direction with span lengths of 22.1 m, 29.5 m and 22.1 m, respectively. The bridge deck is supported by 8 reinforced concrete bridge girders with I-shaped cross sections. The bridge girders are equally distributed in the transverse direction with an interval of 2.419 m.

The bridge superstructure is composed of 8-in concrete slab deck supported by eight parallel pre-stressed concrete I-girders. The girders are reinforced longitudinally at the tops of the cross sections and are braced with stirrups at 18-in intervals. The junctions between adjacent girders, supported by the pier cap, are embedded in a concrete diaphragm creating an integral, fixed connection. Supporting the concrete diaphragms are rectangular pier caps, each supported by an interior and exterior column with constant average depths. Each column contains standard longitudinal reinforcement, and transverse confinement. The abutments and piers are parallel and skewed at the same angle to the transverse axis. The plan and elevation views of the prototype bridge are shown in Fig. 5 a and b, respectively.

3.1.2 Development of a detailed bridge finite element model

The plate element on the bridge has a rectangular shape with the length, width and depth of 0.884 m, 0.914 m, and 0.205 m, respectively. The bridge deck is connected to the bridge girders through rigid link elements. The bridge is supported by gravity abutments at two ends and piers in the middle. The bridge piers are fixed in all directions to the ground. The abutments are restrained in all directions except torsional direction while the piles under the abutments are fixed to the ground. The bridge finite element model in SAP2000 is shown in Fig. 6.

3.1.3 Modal properties of the bridge

The mode shapes and frequency properties are shown in Fig. 7 and Table 1. The bridge motion is dominant in vertical modes for the first 10 modes, which implies that the vertical interaction between bridge and running vehicles could be significant for the bridge performance.

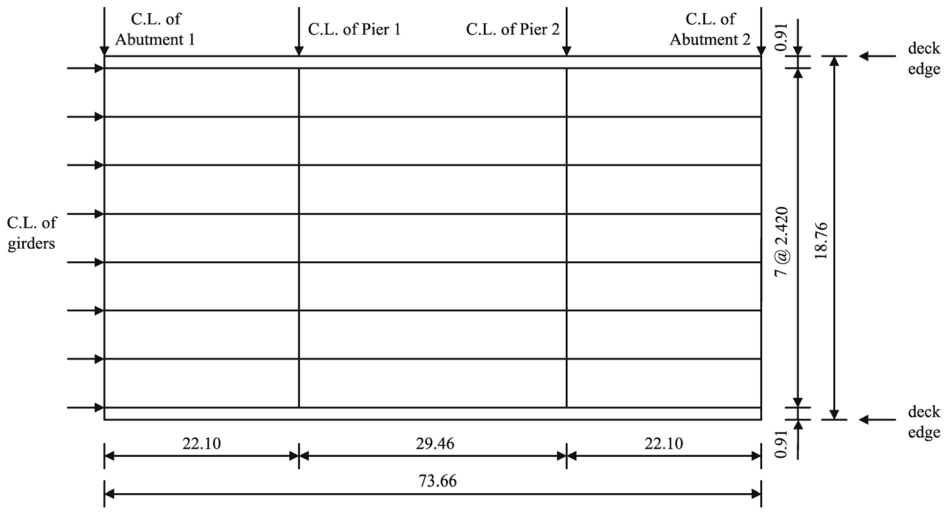

(a) Plan View

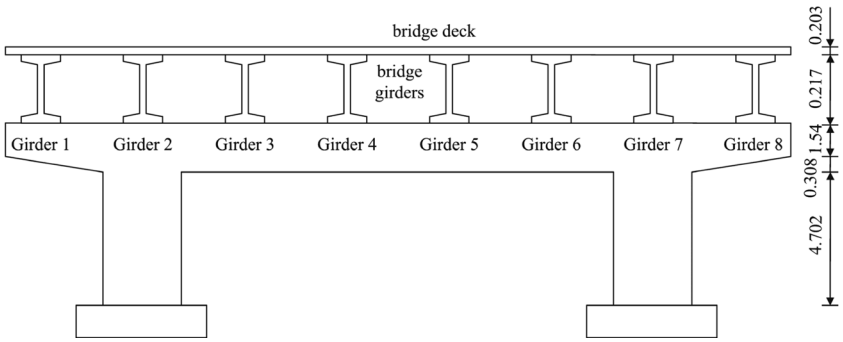

(b) Elevation View

Fig. 5 (**a**) Plan View (**b**) Elevation view of prototype bridge (unit: m)

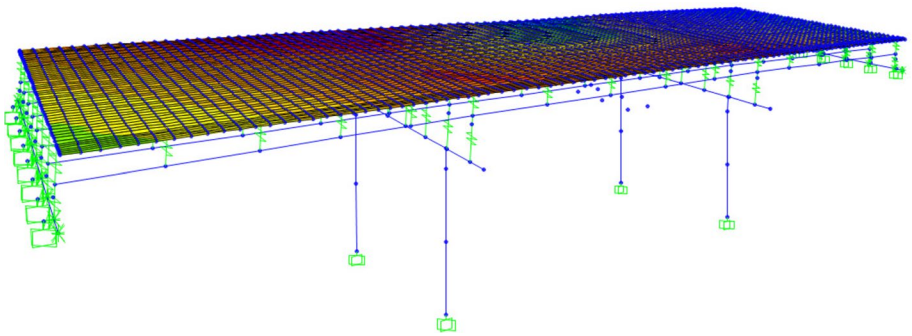

Fig. 6 Bridge finite element model using SAP2000

3.2 Stochastic traffic flow simulation

The stochastic traffic flow is simulated on the three lanes in the same driving direction. The cell length in the cellular automaton model is 7.5 m. The vehicles in the

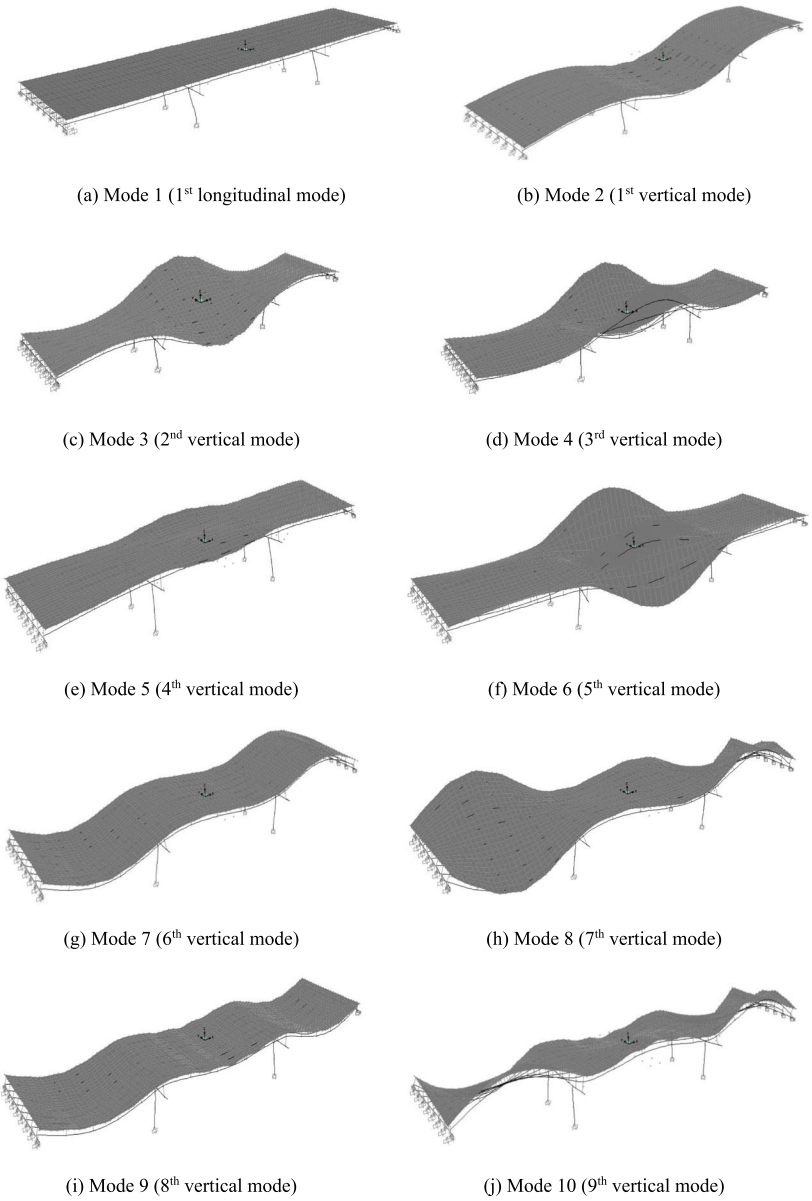

(a) Mode 1 (1st longitudinal mode)

(b) Mode 2 (1st vertical mode)

(c) Mode 3 (2nd vertical mode)

(d) Mode 4 (3rd vertical mode)

(e) Mode 5 (4th vertical mode)

(f) Mode 6 (5th vertical mode)

(g) Mode 7 (6th vertical mode)

(h) Mode 8 (7th vertical mode)

(i) Mode 9 (8th vertical mode)

(j) Mode 10 (9th vertical mode)

Fig. 7 Mode shapes of the first 10 modes of the prototype bridge (scale factor: 60)

traffic flow are categorized as three types, which are light car, light truck, and heavy truck. The vehicle percentages of the baseline scenario for light car, light truck and heavy truck are 50%, 30% and 20%, respectively. The dynamic parameters of each type of vehicles can be found in Zhou and Chen (2015). The stochastic traffic flow is simulated on a roadway-bridge-roadway path to consider the initial dynamic effects of the moving vehicles when they enter the bridge. The roadway segments are assumed to link both ends of the bridge with a length of 75 m each, which is same as the total bridge length. Busy traffic flow is assumed to be present on the bridge with a vehicle density of 33 vehicles/km/lane. The maximum vehicle speed is 30 m/s, which is equal

Table 1 Modal properties of the first 10 modes of the prototype bridge

Mode	Frequency (Hz)	Period (Sec)	Dominant direction	Symmetry
1	1.704	0.587	Longitudinal	Symmetric
2	5.425	0.184	Vertical	Symmetric
3	5.637	0.177	Vertical	Asymmetric
4	6.513	0.154	Vertical	Symmetric
5	7.584	0.132	Vertical	Asymmetric
6	8.175	0.122	Vertical	Symmetric
7	8.428	0.119	Vertical	Asymmetric
8	8.611	0.116	Vertical	Asymmetric
9	9.024	0.111	Vertical	Symmetric
10	9.118	0.110	Vertical	Symmetric

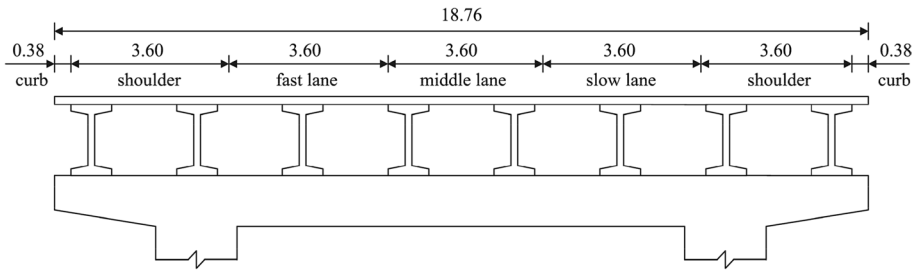

Fig. 8 Location of traffic lanes on the prototype bridge (unit: m)

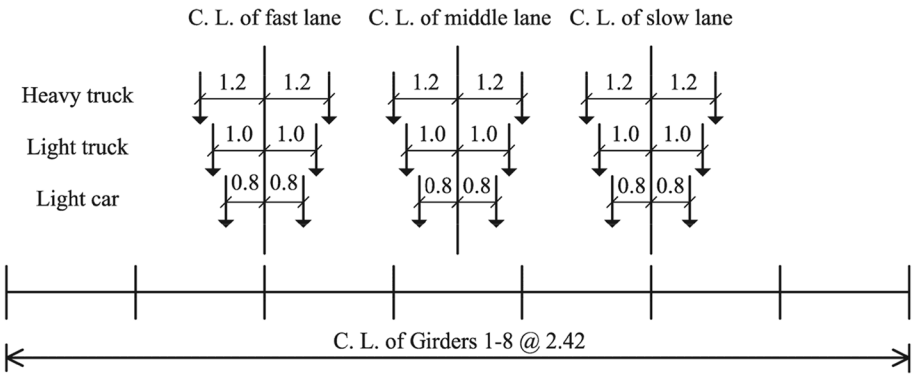

Fig. 9 Wheel location of each type of vehicle on each lane (unit: m)

to 4 times of the cell length. The distribution of three through lanes and their locations on the bridge girders are shown in Fig. 8. The wheel locations from each of the three types of vehicles in each lane are shown in Fig. 9.

The simulated stochastic traffic flow is shown in Fig. 10a, b and c, respectively for the fast lane, middle lane, and slow lane.

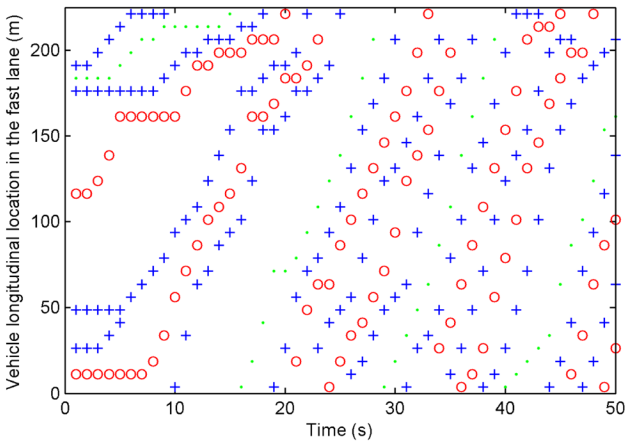

(a) Traffic flow in the fast lane

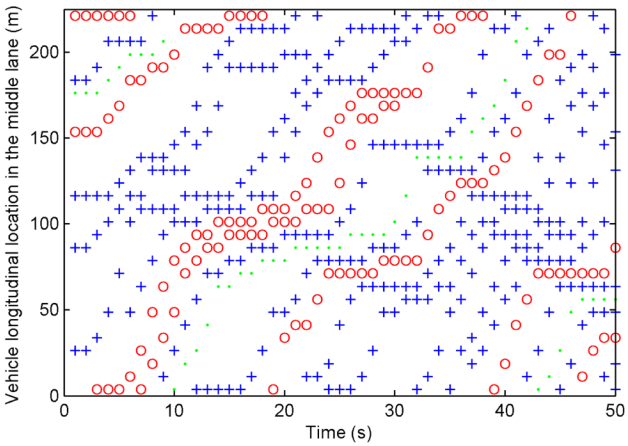

(b) Traffic flow in the middle lane

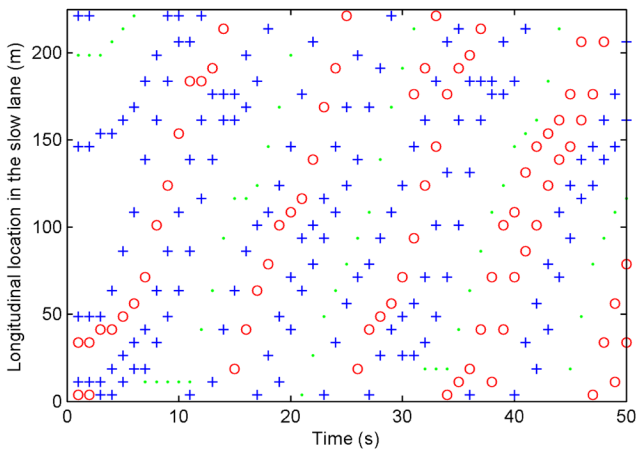

(c) Traffic flow in the slow lane

Fig. 10 Simulated busy traffic flow in the three lanes (· heavy truck; o light truck; + light car)

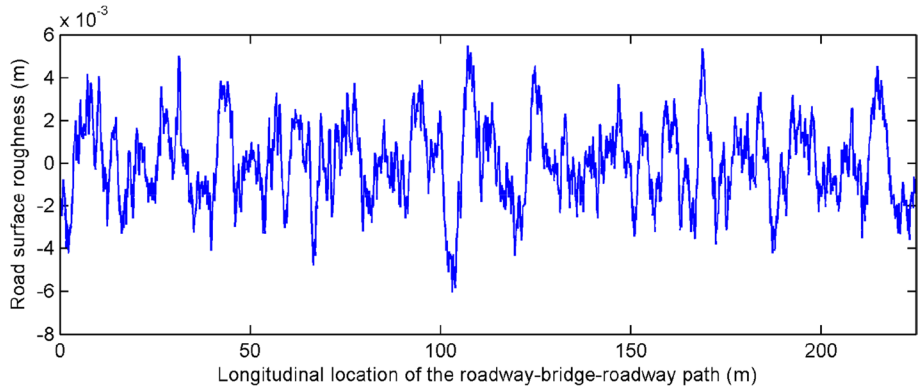

Fig. 11 Road surface roughness in good condition on the simulation path

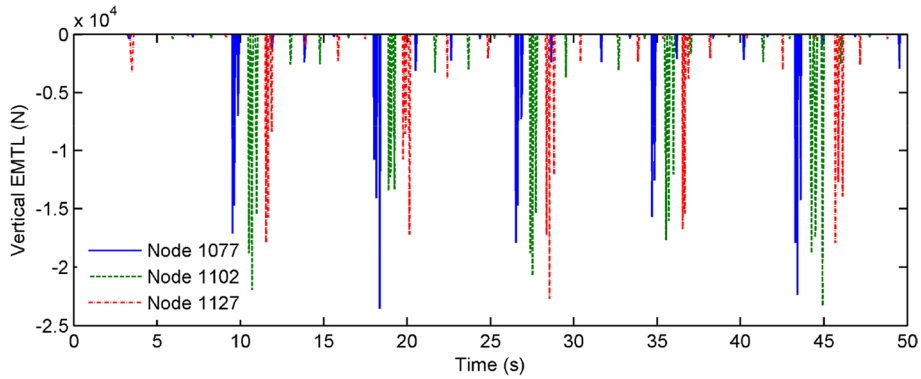

Fig. 12 Time histories of vertical EMTL at representative nodes on the bridge deck

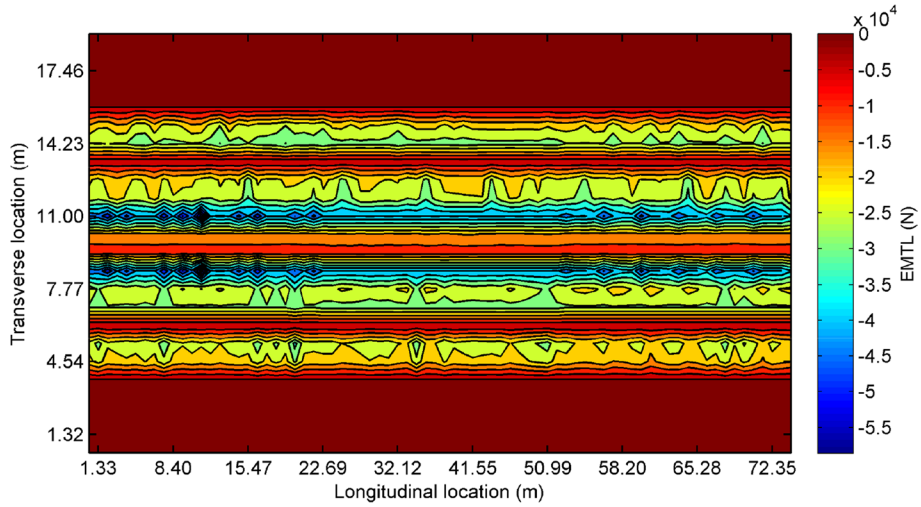

Fig. 13 Filled contour plot of the extreme value of vertical EMTL over the bridge deck

3.3 Simulation of road surface roughness

The road surface is assumed to be in good condition as the baseline scenario, and the surface profile is plotted in Fig. 11. Through the spectral representation approach, road

surface roughness is simulated as a single-variate stationary random process with the road roughness coefficient to be $20 \times 10^{-6}\,\mathrm{m}^3/\mathrm{cycle}$.

3.4 Equivalent moving traffic load (EMTL)

The equivalent moving traffic load (EMTL) on the bridge deck can be obtained from the coupled bridge-traffic interaction analysis results. The time histories of vertical EMTL are obtained at each deck node and those at the representative nodes are shown in Fig. 12. The extreme values of vertical EMTL distributed over the bridge

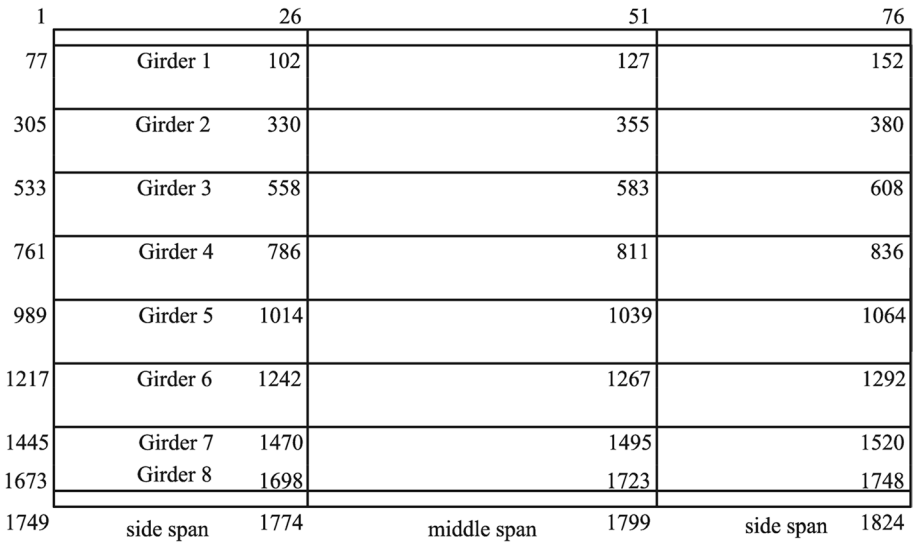

Fig. 14 Node numbers in the bridge deck joints of the bridge model

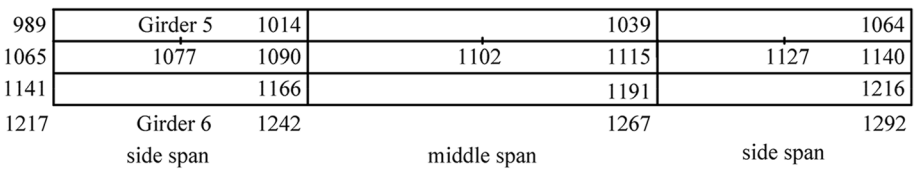

Fig. 15 Locations of representative nodes in each span

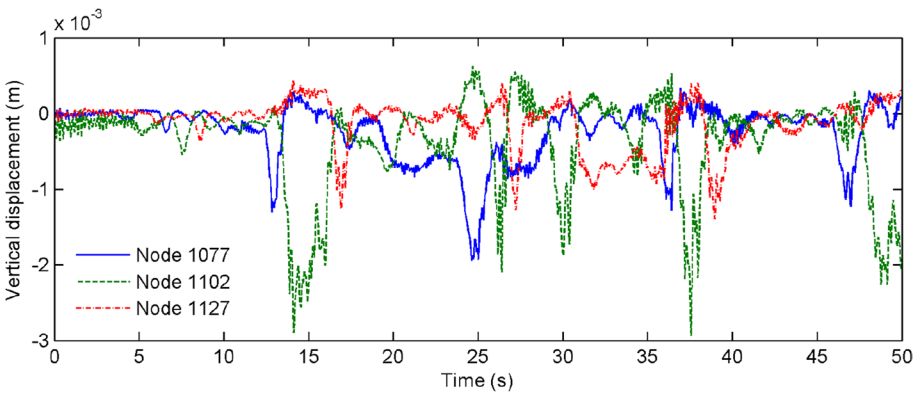

Fig. 16 Vertical displacement response at representative nodes on the bridge deck

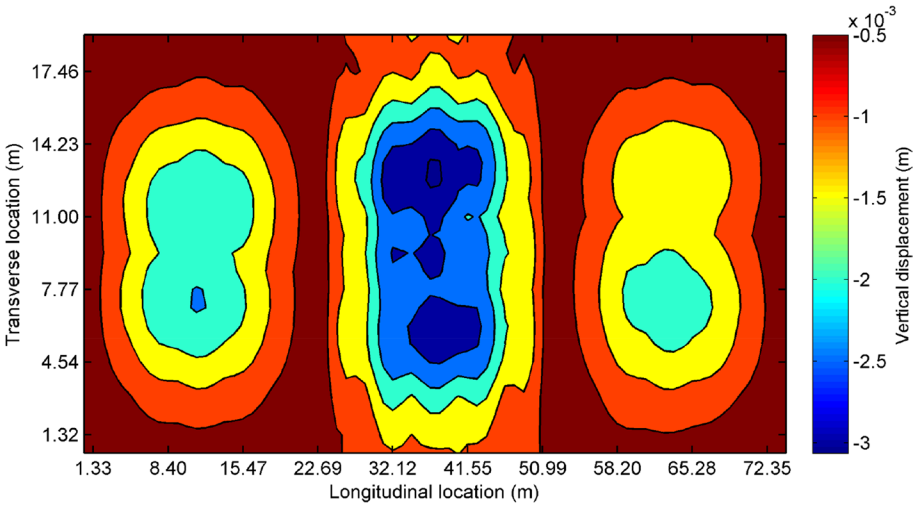

Fig. 17 Filled contour plot of the extreme vertical displacement all over the deck

1		25	26		50	51		75
76	Girder 1	100	101		125	126		150
226		250	251		275	276		300
301	Girder 2	325	326		350	351		375
451		475	476		500	501		525
526	Girder 3	550	551		575	576		600
676		700	701		725	726		750
751	Girder 4	775	776		800	801		825
901		925	926		950	951		975
976	Girder 5	1000	1001		1025	1026		1050
1126		1150	1151		1175	1176		1200
1201	Girder 6	1225	1226		1250	1251		1275
1351		1375	1376		1400	1401		1425
1426	Girder 7	1450	1451		1475	1476		1500
1576	Girder 8	1600	1601		1625	1626		1650
1651	side span	1675	1676	middle span	1700	1701	side span	1725

Fig. 18 Element numbers in the bridge deck of the bridge model

deck are shown in Fig. 13 as a contour plot and the negative sign indicates that the EMTL is downward on the bridge deck.

3.5 Displacement response at the bridge deck

The bridge deck has a total of 1824 nodes and 1725 elements in the refined FE model of SAP2000. The nodes and elements on the bridge deck are numbered according to the grids in the longitudinal direction sequentially. There are 26 nodes on the girder at each span and 4 nodes between two adjacent girder nodes. Therefore, there are 76 nodes for each girder in all the three spans (Fig. 14).

According to the wheel location of vehicles on the lanes in Fig. 9, the representative deck nodes are selected as node 1077, 1102 and 1127 in the left span, middle span, and right span, respectively. The locations of the representative nodes are shown in Fig. 15. The vertical displacement time histories are plotted in Fig. 16 for representative nodes and the contour plot of the extreme vertical displacement all over the deck is shown in Fig. 17. The extreme vertical response is found to increase as the span length increases, and the extreme vertical displacement is largest at the mid span of the longest span (middle span). The fast lane will induce larger vertical response of

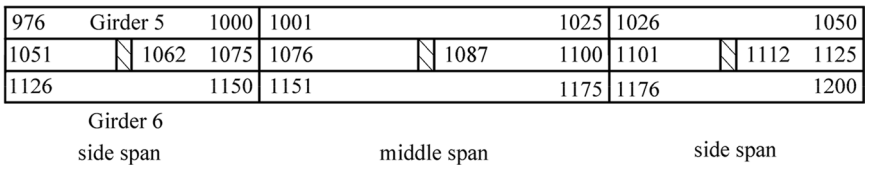

Fig. 19 Locations of representative elements in each span

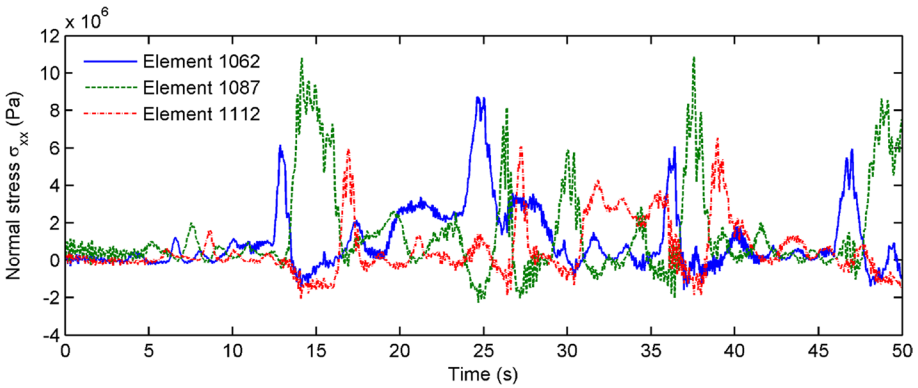

Fig. 20 Principal normal stress (σ_{xx}) of the bottom surface of representative elements on the bridge deck

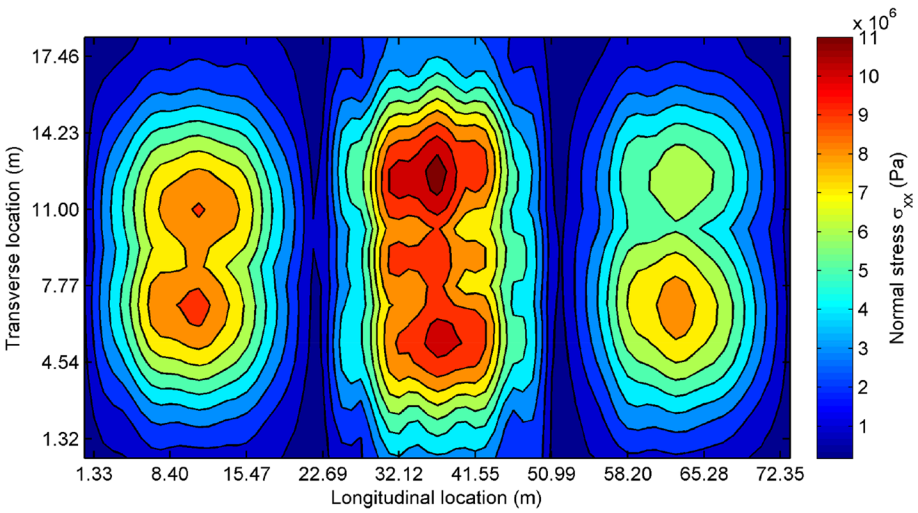

Fig. 21 Extreme positive normal stress (σ_{xx}) of the bottom surface on the bridge deck

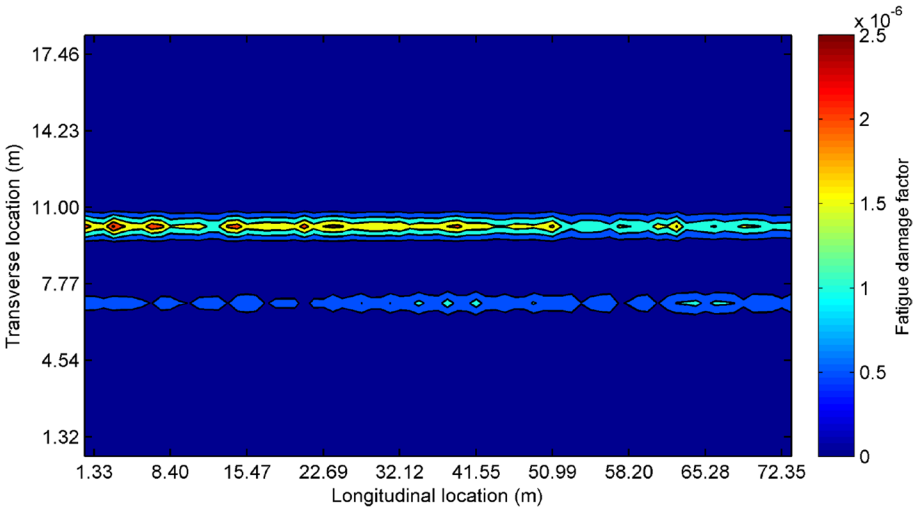

Fig. 22 Fatigue damage factor in 1 hour over the bridge deck

the bridge due to the higher vehicle speeds on average. The randomness of the traffic flow simulation could also play a role in the response difference across the bridge deck.

3.6 Stress response on the bridge deck

The numbers of elements around the representative nodes are shown in Fig. 18 and the bridge deck section between two adjacent girders in each span is divided into 5×3 elements.

The representative deck elements are selected as element 1062, 1087 and 1112 in the left span, middle span, and right span, respectively and the representative elements are marked in Fig. 19.

The time histories of the principle normal stress at the bottom surface of the representative elements on the bridge deck are shown in Fig. 20. The contour plot of the extreme positive value of principle normal stress at the bottom surface all over the bridge deck is shown in Fig. 21. From the hybrid bridge assessment model, detailed displacement and stress response can be obtained on the entire bridge deck, which will provide valuable information in the overall fatigue assessment.

3.7 Fatigue damage prediction on the bridge deck

The main parameters for fatigue damage assessment are listed in this section. The deck depth h is 0.2032 m. The concrete compressive strength $f_c^{'}$ is 4×10^7 Pa. The #4 rebar of ASTM 416 Grade 270 is used with a yield strength of 1.679×10^9 Pa. The diameter and area of the rebar are 0.0127 m and 0.000129 m^2, respectively. For the transverse bars in the main deck direction, on the unit width of b_w, there is a total of 6 tensile rebars and 3 compressive rebars. The neutral axis distance x_m is calculated with the following equation.

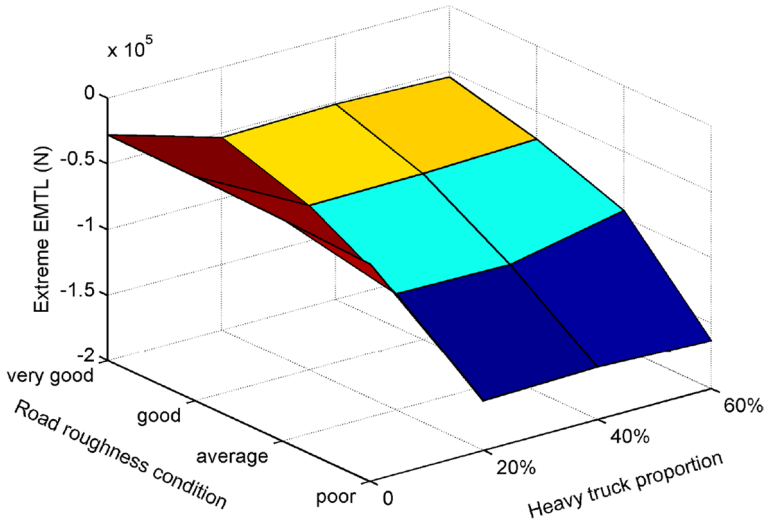

Fig. 23 Extreme EMTL over the bridge deck under different road roughness conditions and vehicle proportions

Table 2 Extreme EMTL values over the bridge deck (unit: N)

Road roughness				
Heavy truck proportion	**Poor**	**Average**	**Good**	**Very good**
None	−34,642	−30,971	−29,145	−27,843
20%	−162,486	−111,478	−74,592	−53,130
40%	−160,068	−112,362	−73,794	−51,178
60%	−163,303	−94,627	−70,710	−54,015

$$x_m = \frac{A_s f_y - A'_s f_y}{0.75 \cdot 0.85 f'_c b_w} \tag{23}$$

By following Eqs. (13–14), the maximum shear and tensile strength of concrete can be calculated. After calculating the punching shear strength with Eq. (12), the fatigue punching shear strength is obtained from Eq. (15), with which the fatigue damage factor in 1 hour can be calculated with Eq. (22). As shown in Fig. 22, the fatigue damage factor has much variation for bridge deck elements on different traffic lanes and the largest fatigue damage factor occurs at the bridge deck elements on the middle lane.

4 Fatigue damage prediction considering different road surface and traffic conditions

The fatigue damage factors are obtained for 12 combinations of road surface conditions and vehicle proportions. Four road surface conditions are involved, which correspond to poor, average, good and very good road conditions with road roughness coefficients of 320E-6, 80E-6, 20E-6 and 5E-6 cycle/m^3, respectively. Three sets of vehicle proportions are considered, in which the proportion of heavy truck is 20%,

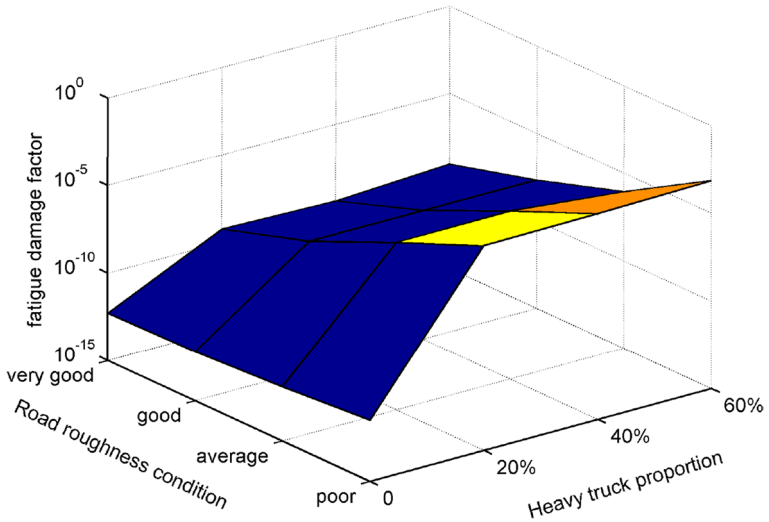

Fig. 24 The maximum fatigue damage factor in 1 hour over the bridge deck under different road roughness conditions and vehicle proportions

Table 3 Maximum fatigue damage factors in 1 hour over the bridge deck (unit: -)

Road roughness				
Heavy truck proportion	**Poor**	**Average**	**Good**	**Very good**
None	3.0308E-12	1.2259E-12	6.4236E-13	5.2996E-13
20%	4.6915E-04	3.7638E-06	2.2570E-08	5.7887E-10
40%	5.4563E-04	4.0905E-06	2.2393E-08	4.0580E-10
60%	7.5356E-04	8.9490E-07	2.1399E-08	8.8256E-10

40% and 60% for set 1, 2 and 3, respectively. In all cases, the proportions of light truck and light car are assigned proportionally in a constant ratio of 3 to 5. Heavy traffic flow is considered with a traffic density of 33 vehicles per kilometer per lane and the speed limit of 30 m/s. The extreme EMTL on the bridge deck for these scenarios are plotted in Fig. 23, where the values are listed in Table 2.

The maximum fatigue damage factor in 1 hour is plotted in Fig. 24 in each scenario corresponding to different road surface conditions and vehicle proportions, with the values listed in Table 3.

The EMTL on the bridge deck increases significantly when heavy trucks are present in the traffic flow. Since limited number of vehicles can be present on the same bridge span at the same time, the extreme EMTL value doesn't have much increase when the proportion of heavy truck is low, e.g., around, or below 20%. Fatigue damage factors increases significantly with deteriorating road surface condition in a logarithmic manner once more heavy trucks are involved in the traffic flow. When heavy truck proportion is below 20%, the differences of fatigue damage factor with different road surface conditions are small. When heavy truck proportion increases beyond 20%, the fatigue damage factor increases significantly when the road surface condition deteriorates. Such increasing trend becomes more significant when the heavy truck

proportion is even higher. It is concluded that the presence of heavy trucks may significantly influence the fatigue life of the bridge RC deck. This is especially true when the road surface condition is not good. Comparatively, the presence of light trucks and light cars pose small risk on the fatigue damage on the bridge deck regardless of the road surface conditions.

5 Conclusions

The study presents a hybrid approach for fatigue assessment of bridge deck considering realistic bridge-traffic interaction. It incorporates the global fully coupled bridge-traffic interaction analysis model, detailed bridge finite element model, and fatigue assessment method directly based on the vehicle loads and shear strength of the bridge deck. It takes advantage of the strength of detailed modeling in commercial finite element software, which provides modal properties of the bridge in plate element scale. Then, the modal properties including the frequencies and modal displacements are used in the fully coupled bridge-traffic interaction analysis to obtain the EMTL acting on different nodes of the bridge deck. The EMTL can be further applied as nodal loads on the finite element model to obtain the local displacement and stress response across the bridge deck. Finally, fatigue assessment is conducted using the EMTL and parameters from the bridge deck to obtain the fatigue damage factors.

The proposed hybrid approach for fatigue assessment on bridge deck is demonstrated on a prototype highway bridge with three spans. First, the EMTL, bridge displacement and stress response and fatigue damage factor are demonstrated for a typical traffic and road surface condition to show the process of the entire simulation platform. Then, the fatigue damage factor is investigated with different road surface roughness and heavy truck proportions. It is found that the presence of heavy trucks may dominantly influence the fatigue life of the bridge RC deck, especially when the road surface condition is not good. It is shown that the presented approach is a powerful tool to obtain detailed bridge deck response and predict fatigue damage considering bridge-traffic interactions.

Acknowledgements
The work presented in this paper was conducted with support from the Mountain-Plains Consortium, a University Transportation Center funded by the U.S. Department of Transportation.

Availability of data and material
The modeling and result data is available upon reasonable request.

Authors' contributions
Yufen Zhou: Conceptualization, Methodology, Investigation, Analysis, Visualization, Writing – original draft. Suren Chen: Conceptualization, Funding acquisition, Supervision, Writing – review & editing.

Funding
Funding was provided by the Mountain-Plains Consortium, a University Transportation Center funded by the U.S. Department of Transportation.

Declarations

Competing interests
There is no competing interest.

Received: 15 November 2023 Accepted: 11 December 2023
Published online: 05 January 2024

References

Cai CS, Chen S (2004) Framework of vehicle–bridge–wind dynamic analysis. J Wind Eng Ind Aerodyn 92(7–8):579–607
Chen SR, Cai CS (2007) Equivalent wheel load approach for slender cable-stayed bridge fatigue assessment under traffic and wind: feasibility study. J. Bridge Eng, ASCE 12(6):755–764
Chen SR, Wu J (2010) Dynamic performance simulation of long-span bridge under combined loads of stochastic traffic and wind. J Bridge Eng, ASCE 15(3):219–230
Deng L, Nie L, Zhong W, Wang W (2020) Developing fatigue vehicle models for bridge fatigue assessment under different traffic conditions. J Bridge Eng, ASCE 26:1–12
Dodds CJ (1972) BSI proposals for generalized terrain dynamic inputs to vehicles. International Organization for Standardization ISO/TC/108/WG9, document no. 5, 1972
González A, Brien O, Cantero EJ et al (2010) Critical speed for the dynamics of truck events on bridges with a smooth surface. J Sound Vib 329(11):2127–2146
Huang D, Wang T-L, Shahawy M (1992) Impact analysis of continuous multigirder bridges due to moving vehicles. J Struct Eng 118(12):3427–3443
Lee HP (1996) Dynamic response of a beam with a moving mass. J Sound Vib 191(2):289–294
Luo Y, Zheng H, Zhang H, Liu Y (2021) Fatigue reliability evaluation of aging prestressed concrete bridge accounting for stochastic traffic loading and resistance degradation. Adv Struct Eng 24(13):3021–3029
MacDougall C, Green MF, Shilinglaw S (2006) Fatigue damage of steel bridges due to dynamic vehicle loads. J. Bridge Eng, ASCE 11(3):320–328
Matsui S (1984) Evaluation of punching shear strength in reinforced concrete decks. Proc JSCE 348(1):133–141
Nassif HH, Liu M (2004) Analytical modeling of bridge-road-vehicle dynamic interaction system. J Vib Control 10(2):215–241
Oh B, Lew Y, Choil Y (2007) Realistic assessment for safety and service life of reinforced concrete decks in girder bridges. J Bridg Eng 12(7):410
Olsson M (1985) Finite element modal co-ordinate analysis of structures subjected to moving loads. J Sound Vib 99(1):1–12
Olsson M (1991) On the fundamental moving load problem. J Sound Vib 145(2):299–307
Paterson W (1986). International Roughness Index: Relationship to other measures of roughness and riding quality. Transp Res Rec 1084–007.
Perdikaris PC, Beim S (1988) RC bridge decks under pulsating and moving load. J Struct Eng 114(3):591–607
Shinozuka M, Jan CM (1972) Digital simulation of random processes and its applications. J Sound Vib 25(1):111–128
Shiyab A (2007) Optimum use of the flexible pavement condition indicators in pavement management system. Ph.D dissertation, Curtin Univ of Technology, Perth, Australia
Wu J, Chen S, van de Lindt JW (2012) Fatigue assessment of slender long-span bridges: reliability approach. J Bridg Eng 17(1):47–57
Xu Y, Guo W (2003) Dynamic analysis of coupled road vehicle and cable-stayed bridge systems under turbulent wind. Eng Struct 25(4):473–486
Yang YB, Wu YS (2001) A versatile element for analyzing vehicle-bridge interaction response. Eng Struct 23:452–469
Yang YB, Yau JD (1997) Vehicle-bridge interaction element for dynamic analysis. J Struct Eng ASCE 123(11):1512–1518
Zhou Y, Chen S (2015) Dynamic simulation of long-span bridge-traffic system subjected to combined service and extreme loads. J Struct Eng ASCE 141(9):04014215
Zhu XQ, Law SS (2002) Dynamic load on continuous multi-lane bridge deck from moving vehicles. J Sound Vib 251(4):697–716

Publisher's Note